Asian Journal of Pharmaceutical Sciences 17 (2022) 867–879

Available online at www.sciencedirect.com

ScienceDirect

journal homepage: www.elsevier.com/locate/AJPS

Original Research Paper

Liposome cocktail activator modulates hepatocytes and remodels the microenvironment to mitigate acute liver failure

Na Yin[a,1], *Wenjun Zhang*[a,1], *Runxiu Wei*[a], *Qiang Yang*[a], *Fengming He*[c], *Ling Guo*[a,b,*], *Min Feng*[a,*]

[a] *School of Pharmaceutical Sciences, Sun Yat-Sen University, Guangzhou 510006, China*
[b] *School of Pharmaceutical Sciences, Hainan University, Haikou 570228, China*
[c] *School of Pharmaceutical Sciences, Xiamen University, Xiamen 361102, China*

ARTICLE INFO

Article history:
Received 16 May 2022
Revised 9 August 2022
Accepted 4 October 2022
Available online 31 October 2022

Keywords:
Cocktail activator
Dimethyl itaconate
Dodecyl gallate
Hepatocyte
Microenvironment modulation

ABSTRACT

Acute liver failure (ALF) is a mortal and critical hepatic disease, in which oxidative stress, inflammation storm and hepatocyte death are crucial in the pathogenesis. Hence, in contrast to the control of a single link, a combination therapy targeting multiple pathogenic links of the disease will be a favorable means to control the progression of the disease. In this study, we constructed dimethyl itaconate-loaded liposomes modified with dodecyl gallate as a cocktail activator to investigate its functional role in acetaminophen (APAP)-induced ALF. Our results demonstrated that the cocktail activator acted on hepatocytes and triggered cocktail efficacy, thereby simultaneously attenuating APAP-induced hepatocyte damage and remodeling the damage microenvironment. The cocktail activator could effectively scavenge reactive oxygen species, inhibit excessive inflammatory responses and reduce cell death in impaired hepatocytes for detoxification. More importantly, the cocktail activator could remodel the damage microenvironment, thus further promoting hepatocyte expansion and specifically switching macrophages from the M1 to M2 phenotype for a favorable liver regeneration of ALF. Furthermore, in APAP-induced ALF mouse model, the cocktail activator improved liver function, alleviated histopathological damage and increased survival rate. In summary, these findings indicate that the cocktail activator may provide a promising therapeutic approach for ALF treatment as a nanomedicine.

* Corresponding authors.
E-mail addresses: guoling7@mail.sysu.edu.cn (L. Guo), fengmin@mail.sysu.edu.cn (M. Feng).
[1] These authors contributed equally to this paper.
Peer review under responsibility of Shenyang Pharmaceutical University.

https://doi.org/10.1016/j.ajps.2022.10.001

1. Introduction

Acute liver failure (ALF) is a rapidly progressive liver injury with a high clinical mortality rate, which is commonly caused by hepatitis virus infection, hepatotoxic drugs and hepatic ischemia-reperfusion injury [1,2]. In particular, acetaminophen (APAP) overdose is a major cause-in-progress for ALF in many countries [3]. APAP in both mice and humans is metabolized by cytochrome P450 enzymes to produce the toxic reactive intermediate *N*-acetyl-p-benzoquinone imine [4,5]. Excessive *N*-acetyl-p-benzoquinone imine formation in APAP overdose depletes the livers antioxidant glutathione and subsequently forms cytotoxic adducts on mitochondrial proteins, ultimately leading to fulminant hepatocyte necrosis and sterile inflammation [6–8]. Generally, oxidative stress, excessive inflammatory response and hepatocyte necrosis play a non-negligible driving role in the occurrence and progression of ALF [9–12]. Since the proteins, lipids and DNA of hepatocytes are cellular structures that are predominantly influenced by reactive oxygen species (ROS), oxidative stress can lead to abnormalities in liver structure and function [13]. Furthermore, the activation of inflammatory responses and the secretion of pro-inflammatory cytokines has been established as a key contributor to hepatocyte injury [7]. Meanwhile, hepatic necrosis reduction and hepatic tissue regeneration were of great significance for regaining hepatic function in ALF patients [1,14]. Hence, mitigation of oxidate stress and suppression of excessive inflammatory responses are extremely essential for the management of ALF.

Nowadays, itaconate has been shown to be a product of mammalian energy metabolism and immune responses, with strong antioxidant effects and anti-inflammatory effects in immune or nonimmune cells [15–17]. Mechanically, itaconate is produced from *cis*-aconitate catalyzed by the enzyme encoded by immune responsive gene 1. Dimethyl itaconate (DMI), as an itaconate's membrane-permeable derivate, has been reported to induce electrophilic stress, react with glutathione and subsequently boost levels of nuclear factor erythroid2-related factor 2 (Nrf2) protein, which in turn initiate expression of downstream antioxidant and anti-inflammatory genes including quinone oxidoreductase-1, heme oxygenase-1 and so on [15,16]. Although over time, it was discovered that DMI cannot be metabolized to itaconate [18]. Nevertheless, it does not detract from the fact that DMI is still a superior Nrf2 activator, as the absence of a negative charge on the conjugated ester group in DMI increases its reactivity towards Michael addition, enabling DMI to be a much more excellent Nrf2 activator than itaconate, similar to the potent Nrf2 activator dimethyl fumarate [16]. The above evidence indicates that DMI is highly promising as a model drug for the treatment of ALF, thereby being selected in our study. As far as we know, there are no researches using DMI to treat APAP-induced ALF and to elucidate the functional role of DMI in it.

Nanoplatform-based targeted drug delivery strategies offer unique advantages for controlling disease progression and remodeling tissue microenvironment [19,20]. Liposomes have been widely used in nanoplatform because they are capable of loading both hydrophilic and hydrophobic drugs, and exhibit good biocompatibility, bioavailability and biodegradability. Simultaneously, liposomes have the ability to be passively targeted and naturally enriched in the liver, making them suitable for liver-targeted delivery in ALF. Moreover, we discovered that dodecyl gallate (DG), a gallic acid ester with a dodecyl fatty acid side chain, has the function of regulating the microenvironment of hepatocytes. When DG was administered to APAP-injured hepatocytes, DG induced high expression of hepatocyte growth factor (HGF), epidermal growth factor (EGF), insulin-like growth factor 1 (IGF-1) and hepatic stimulator substance (HSS) growth factors and IL-4, IL-13, TGF-β and VEGF repair factors in the injured hepatocytes (Fig. 1A-1B). It has been reported that growth factors can promote the regeneration of hepatocytes, while repair factors facilitate the repolarization of macrophages from M1 to M2 [21–27]. Therefore, DG was added to our liposomal delivery system to remodel liver tissue microenvironment. To our knowledge, the efficacy of DG to promote the expression of growth factors as well as repair factors in hepatocytes has not been investigated.

Herein, a cocktail activator-based therapy was proposed to concurrently achieve hepatocyte rescue and microenvironmental modulation (Fig. 1C). In this study, dimethyl itaconate-loaded liposomes modified with DG were successfully fabricated as a cocktail activator (C-activator). The cocktail activator acted on the hepatocytes to arouse the effect of the cocktail, while attenuating APAP-induced hepatocyte damage and remodeling the damage microenvironment. Administration of the cocktail activator reduced oxidative stress, excessive inflammatory responses and cell death in hepatocytes. In the meantime, remodeling of the damage microenvironment by the cocktail activator effectively promoted hepatocyte expansion as well as repolarization of macrophages from the M1 to M2 phenotype. Moreover, *in vivo* experiments illustrated that the cocktail activator displayed excellent therapeutic efficacy and safety in APAP-induced ALF mouse model. Consequently, our research highlights the clinical potential of the cocktail activator as a treatment strategy for ALF.

2. Materials and methods

2.1. Materials

Lecithin (99.8%), dodecyl gallate (DG, 99%) and cholesterol (99%) were obtained from Macklin Reagent Co., Ltd. (Shanghai, China). Dimethyl itaconate (98%) was obtained from Shanghai Yuanye Biochemical Co., Ltd (Shanghai, China). Trichloromethane were sourced from Guangzhou Chemical Reagent Factory (Guangzhou, China). Thiazolyl blue tetrazolium romide (MTT) was purchased from Sigma-Aldrich (USA). Rhodamine B was purchased from Tianjin Municipality Tianxin Superfine Chemical Industry Development Center (Tianjin, China). DMEM Medium, fetal bovine serum (FBS) and Trypsin Parenzyme were obtained from Gibco (Canada). Trizon-RNA extract kit, Evo M-MLV PrimeScript RT reagent kit and SYBR Green Pro-Taq HS qPCR kit were obtained from AG Scientific (USA). DCFH-DA ROS was sourced from Shanghai BestBio Co., Ltd (Shanghai, China).

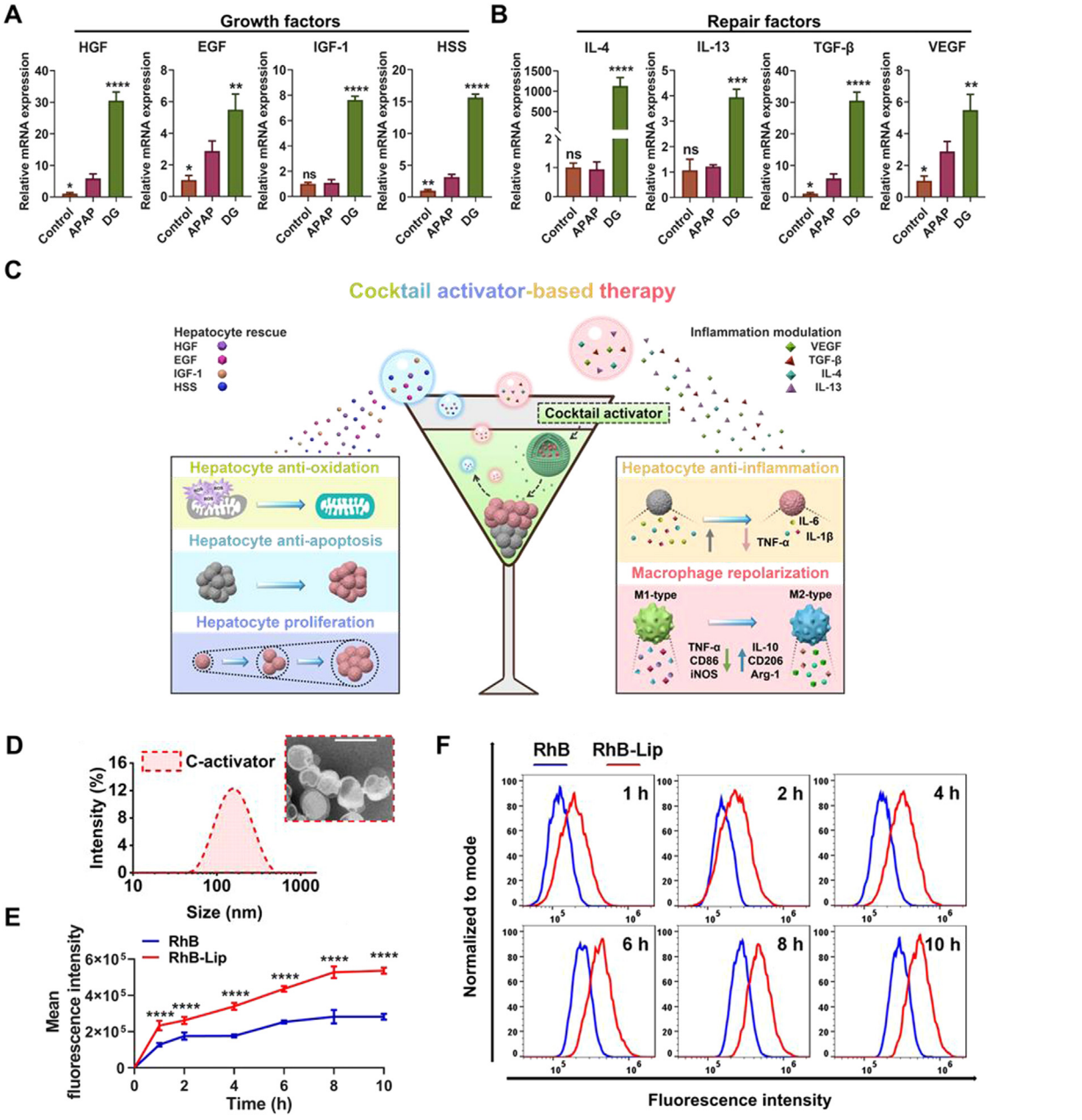

Fig. 1 – Construction and characterization of C-activator. (A) Levels of mRNAs encoding growth factor HGF, EGF, IGF-1 and HSS were quantified using RT-qPCR ($n = 3$; mean ± SD). (B) Levels of mRNAs encoding repair factor IL-4, IL-13, TGF-β and VEGF were quantified using RT-qPCR ($n = 3$; mean ± SD). (C) Schematic diagram of the cocktail activator to realize hepatocyte rescue and inflammation modulation by DMI-loaded liposomes modified with DG. (D) Particle size distribution and TEM image of C-activator. Scar bar is 200 nm. (E-F) Mean fluorescence intensity and flow cytometry graphs of cellular uptake of RhB-Lip (32 μg/ml) by LO2 cells after incubation for 1, 2, 4, 6, 8 and 10 h ($n = 3$; mean ± SD). *$P < 0.05$, **$P < 0.01$, *** $P < 0.001$, **** $P < 0.0001$ compared with APAP group by one-way ANOVA test or two-way ANOVA test.

2.2. *Cell lines and animals*

A murine macrophage cell line Raw-264.7 cells and a human normal liver cell line LO2 cells were obtained from the American Type Culture Collection (ATCC, Manassas, VA, USA). Male BALB/c mice (6–8 weeks old) were sourced from the Laboratory Animal Center of Sun Yat-sen University (Guangzhou, China). The ethical approval number was No.44008500022981. All animal experiments were performed according to protocols approved by the Institutional Animal Care and Use Committee of Sun Yat-sen University (Guangzhou, China).

2.3. *Growth factor and repair factor expression in LO2 cells*

Real-time quantitative PCR (RT-qPCR) was conducted to identify the expression levels of genes related to hepatocyte

growth factor (HGF, EGF, HSS, IGF-1) and repair factor (IL-4, IL-13, TGF-β, VEGF) in APAP-induced LO2 cells damage. LO2 cells were plated in 6-well plates and incubated for 12 h. After that, the medium was replaced with serum-free DMEM medium containing APAP (10 mM) for 3 h. Then the serum-free DMEM medium was discarded and the cells were processed with 10 mM of APAP, 10 mM of APAP + 320 μM DG respectively, for 24 h at 37 °C in 5% CO_2. Subsequently, the total RNA was extracted from LO2 cells sample using Trizon reagent. The RNA was further purified by removing genomic DNA and reverse transcription was carried out using Evo M-MLV RT kit. PCR reactions were conducted using a SYBR Premix Ex Taq II kit in a real-time fluorescent quantitative PCR system (LightCycler 480 II, Roche, Switzerland). The primers for the genes were as follows: HGF: AATCCACTCATTCCTTGGGATT (for), TCCCATTTACAACTCGCAATTG (rev); EGF: GAAGCATT GGACAAGTATGCAT (for), CAGCTTCTGAGTCCTGTAGTAG (rev); HSS: GAGATGATGGACGACCTGG (for), GAGATGATGGAC GACCTGG (rev); IGF-1: AAAAATCAGCAGTCTTCCAACC (for), CCTGTGGGCTTGTTGAAATAAA (rev); IL-4: AAAACTTTG AACAGCCTCACAG (for), GGTTTCCTTCTCAGTTGTGTTC (rev); IL-13: CATGTCCGAGACACCAAAATC (for), CCCTC GCGAAAAAGTTTCTTTA (rev); TGF-β: CTGTACATTGACTT CCGCAAG (for), TGTCCAGGCTCCAAATGTAG (rev); VEGF: ATCGAGTACATCTTCAAGCCAT (for), GTGAGGTTTGATCCGC ATAATC (rev).

2.4. Preparation and characterization of C-activator

Dimethyl itaconate-loaded liposomes modified with DG (C-activator) were prepared using the reverse-phase evaporation method [28]. Briefly, 150 mg lecithin, 50 mg cholesterol, and 10 mg DG were dissolved in trichloromethane (15 ml) and stirred (30 min, 60 °C) to form the oil phase. Then, dimethyl itaconate (30 mg) dispersed in 6 ml PBS as aqueous phase was added dropwise to the polymer solution before sonication for 30 min to produce a stable water-in-oil emulsion. The mixture was immediately transferred to a round-bottom flask and trichloromethane was removed under vacuum with a rotary evaporator at 35 °C till the gel phase disappeared and an aqueous suspension appeared. After that, the aqueous suspension was to hydrate for an additional 1 h, and then an ultrasonic cell crusher (BILON-650Y, Shanghai Bilang Instrument Manufacturing Co., Ltd.) was used to homogenize the resulting mixture (4 min, 30% power, on 1 s, off 1 s) to form the well-proportioned liposomes. Ultimately, the liposomes were filtered using 0.8 μm, 0.45 μm and 0.22 μm syringe millipore membrane successively, and stored at 4 °C for further experiment. Rhodamine B liposomes were prepared using the same method with the aim of comparing the cellular uptake efficiency between free drug and liposome preparation.

Hydrodynamic diameter, polydispersity index (PDI) and zeta potential of C-activator were examined by the dynamic light scattering (Zetasizer Nano ZS ZEN 3600 instrument, Malvern, UK). Stability of C-activator was evaluated for 7 d by measuring the changes in particle size, PDI and zeta potential. The morphology of C-activator was visualized under JEM1400 electron microscope (JEOL, Tokyo, Japan) utilizing negative staining technique using 1% phosphotungstic acid solution.

The encapsulation efficiency (EE) of C-activator were quantified by ultrafiltration centrifugation. The free DMI (non-encapsulated) after separation was detected by a reverse-phase C_{18} column (Cosmosil, 4.6 mm × 250 mm, 5 μm). The flow phase consisted of a mixture of methanol and pH 3.5 phosphate buffer solution (60:40, v/v) and the detection wavelength was 205 nm. Samples were subjected to isopropanol emulsion breaking and then diluted with methanol followed by filtering through a 0.45 μm membrane before injecting samples. The encapsulation efficiency was calculated using the following equation: $EE\ (\%) = W_{\text{liposomes}} / W_{\text{total}} \times 100\%$.

2.5. Cellular uptake of C-activator in vitro

The cellular uptake of C-activator by LO2 cells were determined using flow cytometry. Rhodamine B (RhB) was used as a fluorescence indicator to replace dimethyl itaconate and Rhodamine B-loaded liposomes (RhB-Lip) were prepared using the same method as mentioned above to assess liposomal intracellular uptake [29]. Briefly, LO2 cells were seeded in 12-well plates and then incubated at 37 °C until 60%–80% confluence was reached. Next, the culture medium was replaced with fresh medium containing RhB or RhB-Lip at a final drug concentration of 32 μg/ml and the cells were further incubated for 1, 2, 4, 6, 8 or 10 h respectively. Afterwards, the medium was discarded and LO2 cells were harvested. Subsequently, cells were washed three times with cold PBS and resuspended in PBS for flow cytometry (CytoFLEX, Beckman Coulter, USA).

2.6. Cytotoxicity study

Effect of the liposomes on the viability of LO2 cells was investigated by MTT assays. For this purpose, LO2 cells were seeded into 96-well plates and cultured to reach confluency of 70%. Then LO2 cells were stimulated with 10 mM of APAP diluted with serum-free DMEM medium for 3 h. After that, the medium was discarded and the LO2 cells were treated under the following conditions: Control group (medium only), APAP group (10 mM of APAP), and C-activator group (10 mM APAP + concentrations ranging from 1 to 800 μM of C-activator). MTT solution (5 mg/ml, 10 μl) was added after 24 h and incubated in darkness for another 4 h. Next, 200 μl DMSO was applied to dissolve the formazan crystals. The absorbance at 490 nm was measured using a microplate spectrophotometer (Synergy H1, Bio-Tek, USA).

2.7. Intracellular ROS measurement

Intracellular ROS production was detected by the DCFH-DA fluorescent probe. After LO2 cells were seeded in 12-well plates and cultured overnight, the medium was replaced with serum-free DMEM containing APAP (10 mM) for a 3 h incubation. Then the medium was removed and the LO2 cells were treated according to the following conditions:

Control group (medium only), APAP group (10 mM of APAP), DMI group (10 mM APAP + 400 μM DMI), C-activator group (10 mM APAP + 400 μM C-activator). After 12 h, the medium was abandoned and the LO2 cells were incubated with DCFH-DA fluorescent probe (10 μM) for 30 min at room temperature in the dark. Subsequently, the LO2 cells were visualized with an EVOS® FL Auto Cell Imaging System (EVOS FL, Life Technologies, USA). After that, the LO2 cells were harvested and intracellular ROS levels were measured using a flow cytometry (CytoFLEX, Beckman Coulter, USA).

2.8. *Inflammatory cytokine expression in LO2 cells*

The expression levels of pro-inflammatory cytokine IL-6, IL-1β and TNF-α in LO2 cells after APAP stimulation were measured by RT-qPCR. The culturing conditions and the remainder of experimental procedure was similar to the description mentioned in 2.7. The primers used were as follows: IL-6: CTCCCAACAGACCTGTCTATAC (for), CCATTGCACAACTCTTTTCTCA (rev); IL-1β: TCGCAGCA GCACATCAACAAGAG (for), TGCTCATGTCCTCATCCTGGAAGG (rev); TNF-α: ATGTCTCAGCCTCTTCTCATTC (for), GCTTGTCACTCGAATTTTGAGA (rev).

2.9. *Preparation of conditioned medium (CM)*

For conditioned medium studies, LO2 cells were treated as described in 2.7. Next, the supernatant was collected to obtain the LO2-derived conditioned medium (CM). The supernatant served as control conditioned medium (Ctr CM), APAP conditioned medium (APAP CM), DMI conditioned medium (DMI CM) and C-activator conditioned medium (C-activator CM), respectively.

2.10. *Effect of CM on cell proliferation of LO2 cells*

Crystal violet assay was employed to observe the effect of CM on LO2 cell viability after APAP-induced cell damage. LO2 cells were seeded in 24-well plates overnight. Then LO2 cells were incubated with 10 mM APAP dissolved in serum-free DMEM medium for 3 h. After that, the medium was discarded and LO2 cells in different groups were given the corresponding treatments: Ctr CM group (Ctr CM only), APAP CM group (APAP + APAP CM), DMI CM group (APAP + DMI CM), C-activator CM group (APAP + C-activator CM). After 24 h, the medium was discarded and rinsed twice with PBS followed by staining with 500 μl crystal violet solution for 30 min. The LO2 cells were then rinsed three times with PBS to wash away excess dye. After drying, images were captured with a digital inverted microscope (EVOS, Fisher Scientific, USA). After imaging, methanol (1 ml) was used to dissolve crystal violet and detected at 570 nm by a microplate spectrophotometer (Synergy H1, Bio-Tek, USA).

MTT assay was applied to assess cellular succinate dehydrogenase (SDH) activity after CM treated LO2 cells. LO2 cells were inoculated into 96-well plates and cultured confluency. Then LO2 cells were treated as described above. After 24 h, MTT solution (5 mg/ml, 10 μl) was added and incubated for another 4 h. Then 200 μl DMSO was added and the absorbance at 490 nm was measured using a microplate spectrophotometer (Synergy H1, Bio-Tek, USA).

2.11. *Effect of CM on Raw-264.7 cells survival*

To evaluate the effect of CM on Raw-264.7 cells viability using crystal violet assay. Raw-264.7 cells were seeded to 24-well plates overnight. Subsequently, the medium was substituted with fresh serum-free DMEM containing APAP (10 mM) for 3 h. Afterwards, Raw-264.7 cells were processed for 24 h as follows: Ctr CM group (Ctr CM only), APAP CM group (APAP CM), DMI CM group (DMI CM), C-activator CM group (C-activator CM). Crystal violet assay was performed similarly as 2.10 described.

2.12. *Effect of CM on proinflammatory cytokine expression of Raw-264.7 cells*

To analyze the pro-inflammatory cytokine expression of Raw-264.7 cells after treating with CM, we conducted RT-qPCR to identify the mRNA gene expression. Raw-264.7 cells were incubated for 12 h using 6-well plates. After the medium was aspirated, APAP was dissolved and added in serum-free DMEM at final concentration of 10 mM. After 3 h of incubation, the medium was replaced with Ctr CM, APAP CM, DMI CM, C-activator CM respectively for a 24 h incubation. RNA extraction and RT-qPCR were carried out as described above. The primers used were as follows: IL-10: TTCTTTCAAACAAAGGACCAGC (for), GCAACCCAAGTAACCCTTAAAG (rev); TNF-α: ATGTC TCAGCCTCTTCTCATTC (for), GCTTGTCACTCGAATTTTGAGA (rev).

2.13. *Ability of CM to re-polarize macrophages from M1 to M2 phenotype*

Phenotypic assessment of M1 and M2 macrophages were performed by RT-qPCR following treatment with CM. The dosing, grouping and RT-qPCR were in the same manner described in 2.12 and the primer sequences used were as shown below: CD86: ACGGAGTCAATGAAGATTTCCT (for), GATTCGGCTTCTTGTGACATAC (rev); iNOS: ATCTTGGA GCGAGTTGTGGATTGTC (for), TAGGTGAGGGCTTGGCTGAGTG (rev); CD206: CCTATGAAAATTGGGCTTACGG (for), CTGA CAAATCCAGTTGTTGAGG (rev); Arg-1: CATATCTG CCAAAGACATCGTG (for), GACATCAAAGCTCAGGTGAATC (rev).

2.14. *In vivo therapeutic efficacy*

Acute liver failure was triggered in 6–8 weeks-old male BALB/c mice using overdose acetaminophen (APAP). APAP (30 mg/ml) was dissolved in saline at 60 °C and maintained in a water bath until use. The mice were randomly assigned into four groups (Control group, APAP group, DMI group, C-activator group), and fasted overnight for approximately 16 h prior to inject intraperitoneally with 300 mg/kg APAP except normal group. After 3 h, each group received one of the following treatments by intraperitoneal injection: (1) Control group (saline); (2) APAP group (saline); (3) DMI group (DMI); (4) C-activator group (C-activator). DMI group and C-activator group

were administrated at the equivalent dose of 50 mg/kg DMI per mouse.

The body temperature and survival rate of the mice were recorded during experiment. The mice were sacrificed 24 h after administration to harvest blood sample and weigh their organs. The ratio of the weight of each organ (heart, liver, spleen, lung or kidney) to its body weight in experimental animals, the organ index, was recorded. The gross appearance of liver from each group was photographed. Then livers were decalcified, paraffin-embedded and sectioned for hematoxylin and eosin (H&E) staining. The blood samples were allowed to stand at room temperature for 6 h and then centrifuged. After that, serum was collected to analyze by Automatic Biochemical Analyzer (HITACHI, Japan). Biochemical parameters include serum alanine aminotransferase (ALT), aspartate aminotransferase (AST), alkaline phosphatase (ALP) and total bilirubin (TBIL). The determination of malondialdehyde (MDA) content in the liver tissues was performed by thiobarbituric acid method using an MDA assay kit (Beyotime Institute of Biotechnology, shanghai, China).

2.15. *Statistical analysis*

All of the data were expressed as mean ± standard deviation (SD). The unpaired Student's two-tailed *t*-test was used to compare the mean between two independent groups and ordinary one-way (or two-way) ANOVA with a Tukey's test or Dunnett's test were performed for multiple group comparisons by GraphPad Prism 9.0 (GraphPad, San Diego, CA, USA). A threshold less than 0.05 was considered statistically significant.

3. Results and discussion

3.1. *Characterization and in vitro cellar uptake of C-activator*

The drug delivery efficacy of liposomes may be influenced by numerous factors [30]. Therefore, we first prepared C-activator by applying two different methods, the thin-film hydration method and the reverse evaporation method, respectively. It was noticed that due to the strong water solubility of DMI, the encapsulation efficiency obtained by applying the reverse evaporation method was remarkably higher than that of the thin-film hydration method, and thus the reverse evaporation method was finally selected (Table S1). Subsequently, the C-activator were characterized for size, size distribution, zeta potential, encapsulation efficiency and stability. The results showed that the diameter of C-activator measured by dynamic light scattering was 173.6 ± 2.6 nm. It has been reported that nanoparticles with diameters of 150–300 nm may be mainly located in the liver and spleen, thereby the particle size of C-activator was favorable for liver-targeted delivery [31]. Furthermore, TEM results demonstrated that the morphology of C-activator was homogeneous and spherical, with a typical phospholipid bilayer structure (Fig. 1D). The polydispersity index (PDI) of C-activator was 0.191 ± 0.032, indicating a rather uniform size distribution. Moreover, the zeta potential and encapsulation efficiency of C-activator were −11.9 ± 1.6 mV and 45.59% ± 4.76%, respectively. The stability of liposomes is an important indicator to measure the quality of the formulation. As illustrated in Fig. S1 and S2, no significantly change was observed in the size, PDI and zeta potential of C-activator within 7 d of storage at 4 °C (Fig. S1A- S1B and Fig. S2A- S1B).

To assess the enhanced uptake of C-activator by hepatocytes, LO2 cells (a human normal hepatocyte cell line) were utilized as a hepatocyte model *in vitro*. The cellular uptake characteristics of C-activator in LO2 cells were evaluated by flow cytometry, using Rhodamine B (RhB) as a fluorescence marker. The results indicated that RhB-Lip robustly increased fluorescent signals of RhB in LO2 cells compared with free RhB at different times. In addition, the cellular uptake efficiency of RhB-Lip increased rapidly from 1 h to 10 h, reflecting the time-dependent uptake of RhB-Lip by LO2 cells (Fig. 1E-1F). The increased cellular uptake may be the result of drug encapsulation into liposomes, which enhances the transmembrane properties and intracellular accumulation of hydrophilic drugs [32,33].

3.2. *Evaluation of the actions of C-activator against APAP-induced hepatocyte injury*

In ALF, hepatocyte death, oxidative stress and cytokine storms are the main reasons for the uncontrolled deterioration of the disease [34–37]. Hence, we studied the influence of the cocktail activator on APAP-induced hepatocyte injury from the above three aspects. First, the cytoprotective effect of the cocktail activator against APAP in LO2 was investigated by MTT assay. The results implied that the cocktail activator dramatically reduced the APAP-induced cytotoxicity and improved the viability of hepatocytes in a dose dependent manner (Fig. 2A). Considering that oxidative stress plays an essential role in ALF, the ROS scavenging capability of the cocktail activator was further examined. Mitochondrial membranes are important sources of ROS. The ROS probe DCFH-DA was applied to measure the level of intracellular ROS by digital inverted microscope and flow cytometer. As anticipated, the intracellular ROS generation was notably increased after APAP stimulation, which was dramatically reversed by the cocktail activator (Fig. 2B). Similar results were also observed by the quantitative flow cytometry analysis. Meanwhile, the level of ROS in the C-activator group was significantly lower than that in the DMI group, which was attributed to the increased DMI uptake by hepatocytes in the C-activator group (Fig. 2C-2D). Subsequently, the effect of the cocktail activator on the APAP-induced pro-inflammatory cytokine production in hepatocytes was evaluated. The RT-qPCR analysis illustrated that the expression levels of IL-6, IL-1β and TNF-α were markedly up-regulated in LO2 cells stimulated by APAP. However, the cocktail activator drastically down-regulated the production of IL-6, IL-1β and TNF-α, in sharp contrast to the pro-inflammatory cytokine levels in the APAP group. What's more, free DMI also suppressed the production of pro-inflammatory cytokine, but to lesser extent than the cocktail activator (Fig. 2E-2G and Fig. S4A- S4B). The above evidence clearly indicated that the cocktail activator could ameliorate APAP-induced hepatocyte injury by modulating cell death,

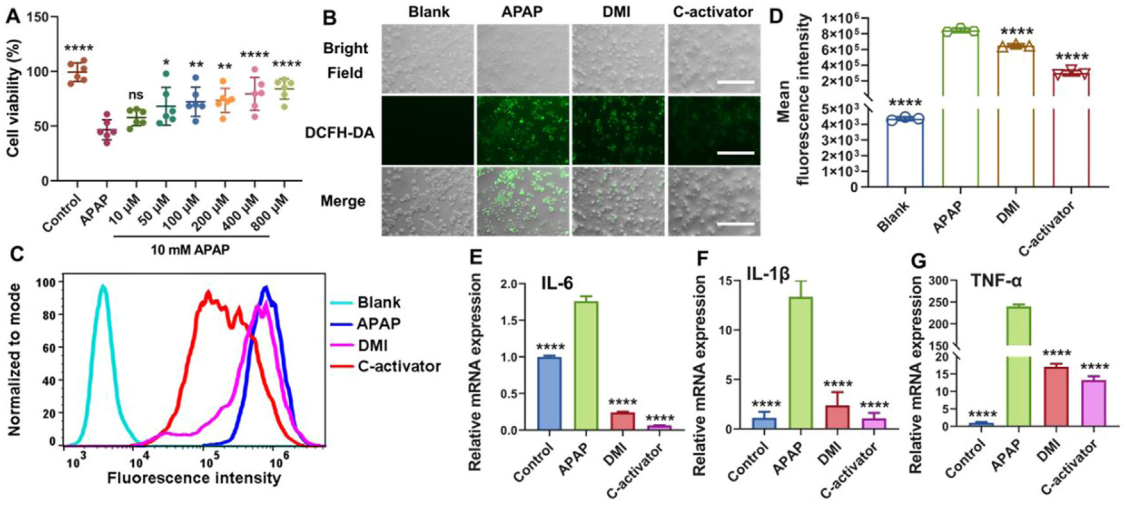

Fig. 2 – *In vitro* cell viability, antioxidant activities, and anti-inflammatory properties of C-activator in APAP-injured LO2 cells. (A) Cell viability of LO2 cells exposure to C-activator in the presence of APAP (10 mM) for 24 h ($n = 6$; mean ± SD). (B) Confirmation of generation and inhibition of ROS in LO2 cells undergoing C-activator treatment, scale bars are 400 μm. (C-D) Intracellular generation of ROS in LO2 cells detected by flow cytometry using DCFH-DA probe ($n = 3$; mean ± SD). (E-G) Total RNA extracted from LO2 cells was measured by RT-qPCR and the expression levels of proinflammatory cytokines IL-6, IL-1β and TNF-α were normalized to the mRNA level of β-actin ($n = 3$; mean ± SD). *$P < 0.05$, **$P < 0.01$, ****$P < 0.0001$ compared with APAP group by one-way ANOVA test.

oxidative stress and inflammation. The mechanism of above actions might be attributed to Nrf2-mediated antioxidative response activated by IRG1/itaconate pathway in hepatocytes [17]. Nrf2 is a ubiquitously expressed transcription factor that protects against oxidative stress. Under normal physiological conditions, Nrf2 binds to Kelch-like ECH-associated protein 1 (Keap1) in the cytoplasm, which makes Nrf2 in a functionally inhibited state. [38]. Among environmental oxidative or electrophilic stresses, Nrf2 is uncoupled from Keap1 into the nucleus, where it binds to the DNA sequence of the antioxidant response element, and initiates the expression of antioxidant and anti-inflammatory target genes, including HO-1, NQO1 and others [39,40]. Many studies have identified that Nrf2 depletion increases susceptibility to toxin-induced liver injury, all of which provide strong evidence for Nrf2 as a hepatoprotective pathway [41–43]. In general, itaconate is considered to be an immunomodulator of macrophages [15,16]. Our study expands on the significance of itaconate in nonimmune cells and identifies itaconate as a promising therapeutic strategy for APAP-induced hepatocyte injury.

3.3. *Microenvironment of C-activator-treated hepatocytes induces hepatocyte expansion in vitro*

The tissue microenvironment is critical determinant of the function of hepatocytes [44,45]. To further evaluate the role of the cocktail activator on tissue microenvironment, we established a model of hepatic injury in LO2 cells with APAP to mimic the microenvironment of ALF model *in vitro*. After a 3 h incubation with APAP, PBS, DMI or C-activator were added into the supernatant and LO2 cells were cultured for another 24 h to achieve control conditioned medium (Ctr CM), hepatocyte injury conditioned medium (APAP CM), DMI-treated hepatocyte injury conditioned medium (DMI CM), and C-activator-treated hepatocyte injury conditioned medium (C-activator CM). Then, the conditioned medium was transferred to APAP-treated LO2 cells for 24 h to investigate the effect of the microenvironment on hepatocyte expansion (Fig. 3A). Crystal violet assay and MTT assay were applied to examine cell viability and succinate dehydrogenase (SDH) activity of LO2 cells, respectively. The results revealed that the morphology of LO2 cells changed significantly after APAP CM treatment, becoming shuttle-shaped compared with the original triangular or hepatic plate-like shape of hepatocytes, and the cell viability was reduced to approximately 50% of that of the Ctr CM group. Surprisingly, the C-activator CM induced nearly 2-fold hepatocyte proliferation compared with the APAP CM and approached the control level. Furthermore, treatment with C-activator CM restored the morphology of LO2 cells to that of normal hepatocytes. However, there was no remarkable difference in hepatocyte viability between the DMI CM group and the APAP CM group (Fig. 3B-3C). Likewise, the MTT assays also demonstrated similar results (Fig. 3D). The amount of residual drug substance in the CM was measured to rule out the possibility of the direct impact of drug substance on these cells. The results showed that the residual percentage of dimethyl itaconate in the C-activator group and the DMI group were about 6.34% ± 0.33% and 8.61% ± 0.48%, respectively, which were much less than the minimum effective concentration (Fig. S3 and Fig. 2A). As we all know, HGF, EGF, IGF-1 and HSS trigger a proliferative response in hepatocytes and mediate hepatic regeneration after liver injury [21–26]. Since the DMI CM group did not show the promotion of hepatocyte proliferation, whereas the C-activator CM group showed a remarkable proliferative effect,

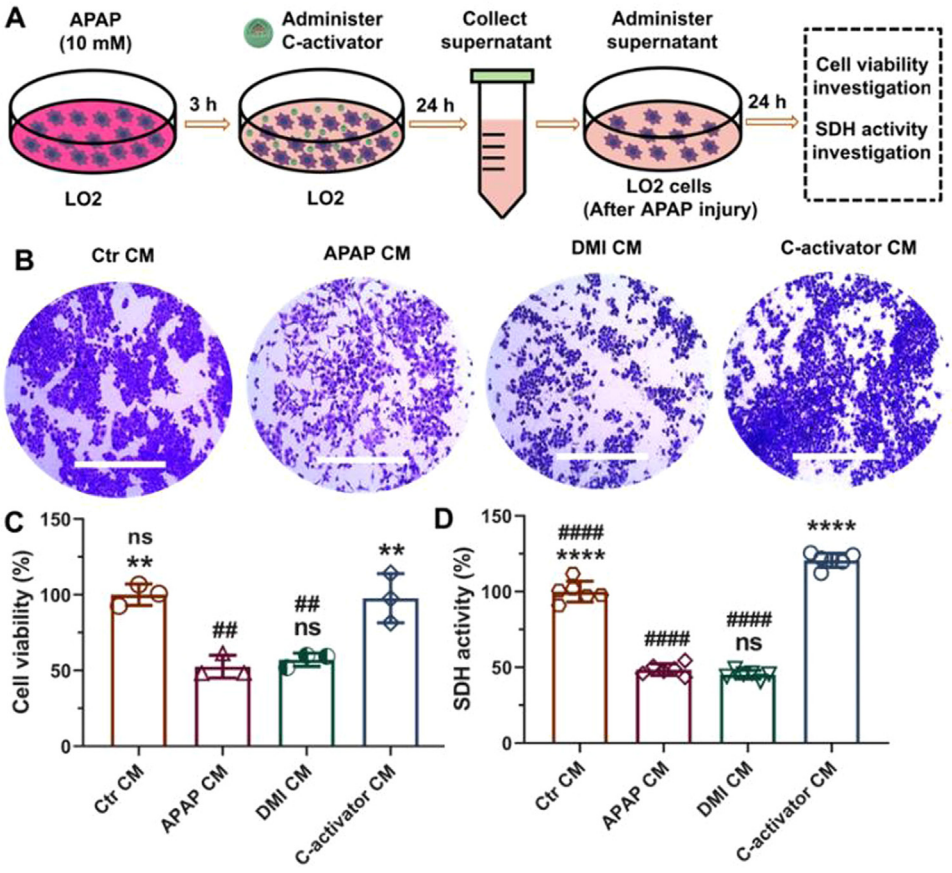

Fig. 3 – C-activator conditioned medium enhanced cell viability after APAP-induced hepatocyte damage. (A) A schematic illustrating the experimental protocol for conditioned medium (CM) administration. (B-C) Cell viability of LO2 cells treated with different CM was evaluated by crystal violet staining and quantified by measuring the absorbance at 570 nm ($n = 3$; mean ± SD). (D) Succinyl dehydrogenase (SDH) viability of LO2 cells treated with CM was measured using MTT assay ($n = 6$; mean ± SD). $^{**}P < 0.01$, $^{****}P < 0.0001$ compared with APAP CM group by one-way ANOVA test and $^{\#\#}P < 0.01$, $^{\#\#\#\#}P < 0.0001$ compared with C-activator CM group by one-way ANOVA test.

we hypothesized that the proliferative effect of C-activator CM was mainly attributed to the existence of DG, which was also consistent with our previous experimental results. For our proof-of-concept, Fig. 1A showed that DG markedly increased the production of HGF, EGF, IGF-1 and HSS relative to the APAP group. Hence, DG was able to increase the content of growth factors in the APAP-injured microenvironment, which in turn promoted hepatic regeneration by modulating the microenvironment. There is no research report that DG can promote the expression of hepatocyte growth factor under the condition of APAP injury, and the specific mechanism needs to be further demonstrated in future research.

3.4. *Microenvironment of C-activator-treated hepatocytes induces anti-inflammatory effects and repolarization of macrophages in vitro*

Activation of immune mechanisms that enhance inflammation after the initial insult can result in a lethal loss of hepatic function due to increased cell death [1]. In ALF, the liver is infiltrated by activated macrophages and various immune cells, which can cause inflammatory storms and induce fulminant liver failure [46]. Activated macrophages, known as M1 macrophages, can act as drivers of ALF progression by producing numerous pro-inflammatory cytokines such as TNF-α [47]. On the contrary, macrophages participating in inflammatory suppression, tissue repair and tissue structural reconstruction are thought to be of the M2 phenotype [48]. Thus, switching predominant M1 phenotype macrophages in ALF to M2 phenotype is very valuable in controlling the disease progression of ALF. Next, the effect of the microenvironment of C-activator-treated hepatocytes on macrophages was investigated. Briefly, Ctr CM, APAP CM, DMI CM or C-activator CM were applied to Raw-264.7 cells to examine the impact of each group of conditioned medium on macrophage survival, inflammatory cytokine expression and macrophage phenotype (Fig. 4A). Crystal violet cell proliferation assay demonstrated that C-activator CM had no significant impact on the growth of Raw-264.7 cells (Fig. 4B). Furthermore, TNF-α mRNA levels isolated from macrophages after being treated with C-activator CM were much lower than those treated with APAP CM (Fig. 4C). Conversely, C-activator CM dramatically increased the production of IL-10, in sharp contrast to the expression in the APAP CM-treated

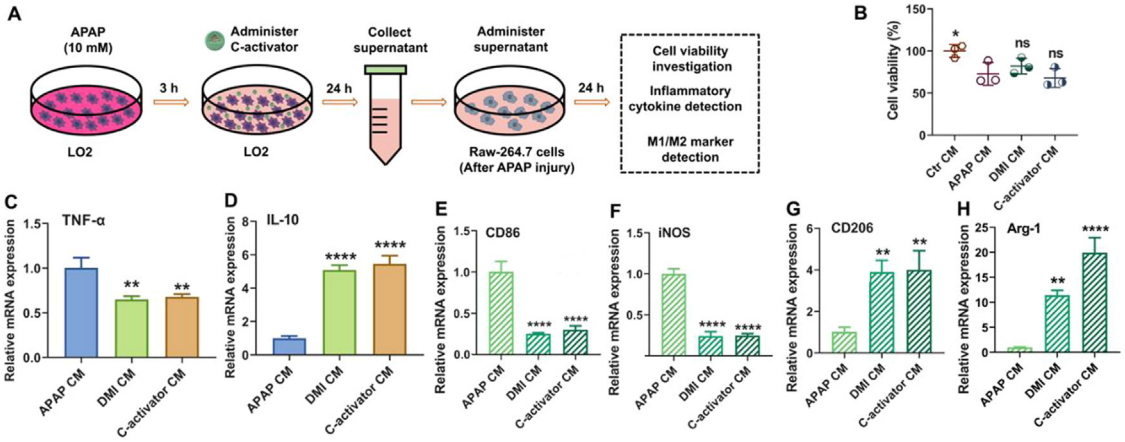

Fig. 4 – Effects of C-activator conditioned medium on Raw-264.7 cells survival, inflammatory cytokine levels and M1/M2 phenotype macrophage regulation. (A) Schematic of CM administration to Raw-264.7 cells. (B) Quantification of cell viability after treatment with different CM were assessed based on crystal violet absorbance at 570 nm ($n = 3$; mean ± SD). (C-D) The mRNA levels of TNF-α and IL-10 were analyzed by RT-qPCR ($n = 3$; mean ± SD). (E-H) The mRNA levels of M1 macrophage phenotype markers (CD86 and iNOS) and M2 macrophage phenotype markers (CD206 and Arg-1) were analyzed by RT-qPCR ($n = 3$; mean ± SD). *$P < 0.05$, **$P < 0.01$, ****$P < 0.0001$ compared with APAP CM group by one-way ANOVA test.

group (Fig. 4D). Then, the changes in M1 markers (CD86 and iNOS) and M2 markers (CD206 and Arg-1) in Raw-264.7 cells treated with various conditioned medium were measured [49]. The results suggested that C-activator CM strongly down-regulated the expression of CD86 and iNOS compared with APAP CM (Fig. 4E-4F). At the same time, C-activator CM up-regulated the levels of CD206 and Arg-1 more than the other groups (Fig. 4G-4H). The possible reason was that DMI suppressed the levels of pro-inflammatory cytokines and DG increased the levels of repair factors in the hepatocyte microenvironment (Fig. 1B and Fig. 2E-2G). Overall, the above evidence clearly revealed that the microenvironment of C-activator-treated hepatocytes could effectively reprogram macrophages with M1 phenotype to M2 phenotype, and inhibit the production of pro-inflammatory cytokines while promoting the production of anti-inflammatory cytokines.

3.5. *The cocktail activator shows enhanced therapeutic efficacy in APAP-induced acute liver failure mouse model*

In this essay, we applied an ALF mouse model caused by injection of APAP at a sublethal dose of 300 mg/kg into male BALB/c mice to investigate the therapeutic efficacy of the cocktail activator. Mice were fasted for 16 h prior to APAP injection to reduce the glutathione concentration and amplify the overdose effect of APAP [50]. Next, mice were randomly distributed into several groups. One group was used as the control, and the mice in treatment groups were intraperitoneally injected with APAP, then respectively subject to treatment with PBS, free DMI or C-activator at 3 h post APAP injection, and fasted throughout (Fig. 5A). Representative photographs taken of the liver morphology showed that APAP induced liver congestion and increased roughness. Strikingly, these symptoms disappeared after the treatment of the cocktail activator, indicating the high efficacy of the cocktail activator in ALF treatment. In contrast, free DMI treatment lacked in liver targeting and accumulation ability, resulting in a relatively weak therapeutic effect (Fig. 5B). Furthermore, the organ index of liver is a good indicator of the degree of liver hyperemia and edema. A remarkable increase in the organ index of liver was noticed in the APAP group compared with the control group, while no obvious difference was observable between the cocktail activator group and the control group (Fig. 5C). What's more, increased treatment efficiency was associated with improvements in animal behavior, such as core body temperature. The body temperature of mice continued to decrease after APAP treatment as the disease progressed, while this progression was nearly blocked in the mice treated with the cocktail activator (Fig. 5D-5E). Besides, whether the cocktail activator could promote the survival of mice subjected to a sublethal dose of APAP was investigated. As illustrated in Fig. 5F, compared with the APAP group, the cocktail activator conferred a significantly higher survival rate of ALF mice. Additionally, malondialdehyde (MDA) is one of the metabolites of lipid peroxidation reactions and its level reflects the content of free radicals in tissues [51]. The data suggested that APAP markedly increased liver tissue MDA levels compared with the control group, whereas the cocktail activator drastically relieved liver damage and decreased MDA levels compared with the moderate inhibitory effect of free DMI (Fig. 5G).

When the liver is damaged, serum levels of ALT, AST, ALP and TBIL are elevated because the enzymes are released from the impaired liver into the bloodstream [52]. To further confirm the therapeutic effectiveness, the levels of the above four biomarkers in serum were measured. As reflected in Fig. 6A-6D, APAP-treated mice reflected a sharp increase in these biomarkers of liver injury after APAP intoxication. However, treatment of the cocktail activator was effective to suppress ALT, AST, ALP and TBIL levels. Additionally, the histological analysis of the liver dissected from the PBS, APAP, DMI and C-activator-treated mice was conducted. The

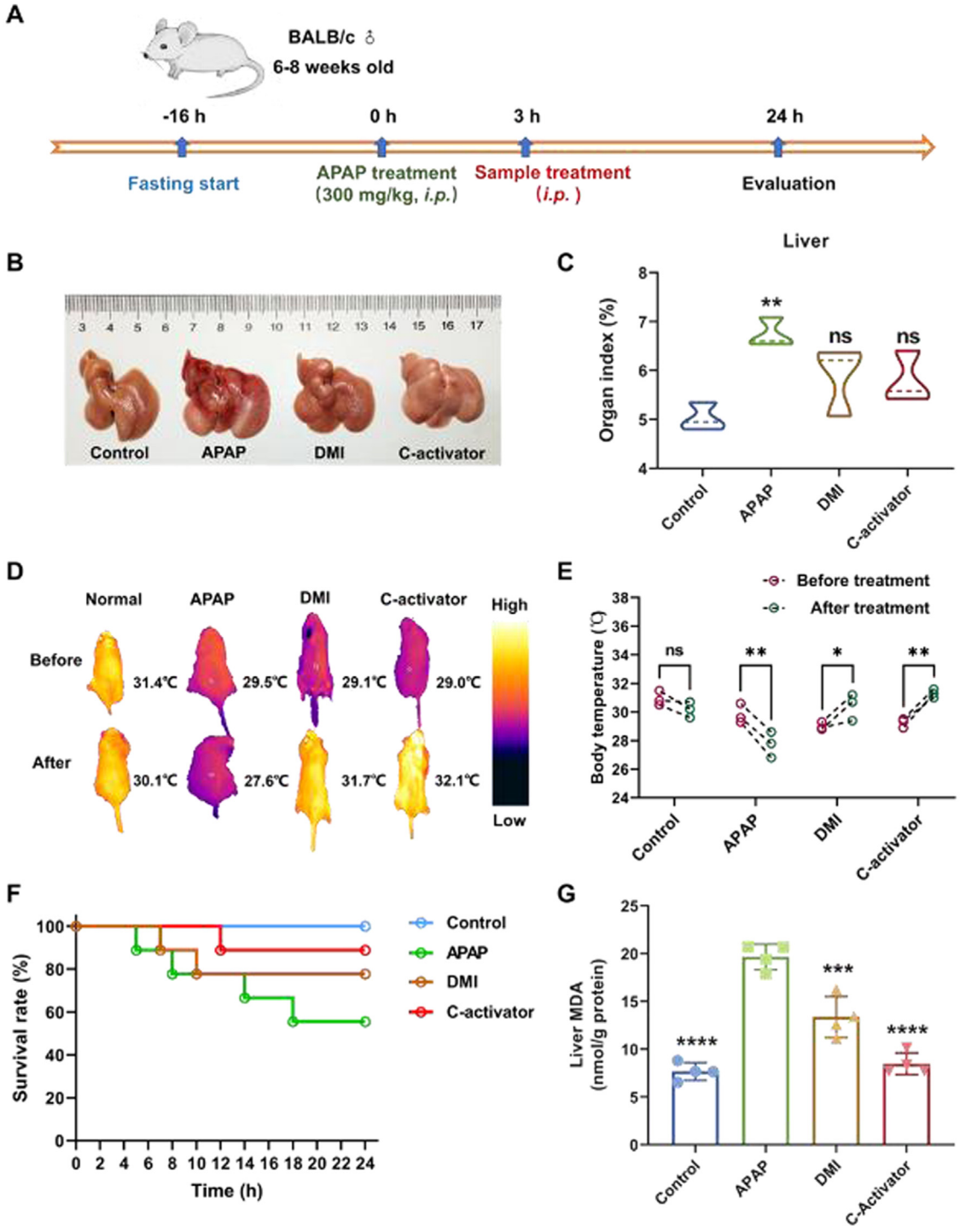

Fig. 5 – *In vivo* therapeutic efficacy of C-activator in APAP-induced ALF mouse model. (A) Schematic diagram of APAP induction and treatment protocol. (B) Representative photographs of livers from different groups at 24 h after APAP injection. (C) Liver-to-body weight ratio from each group ($n = 3$; mean ± SD; comparison with control group). (D-E) Representative pictures and quantification showing the change of each mouse on body temperature before and after treatment ($n = 3$; mean ± SD). (F) Kaplan-Meier survival curves of mice with ALF under various treatments ($n = 10$ per group). (G) MDA content of liver tissues of each group ($n = 4$; mean ± SD; comparison with APAP group). * $P < 0.05$, ** $P < 0.01$, ***$P < 0.001$, ****$P < 0.0001$ by one-way ANOVA test.

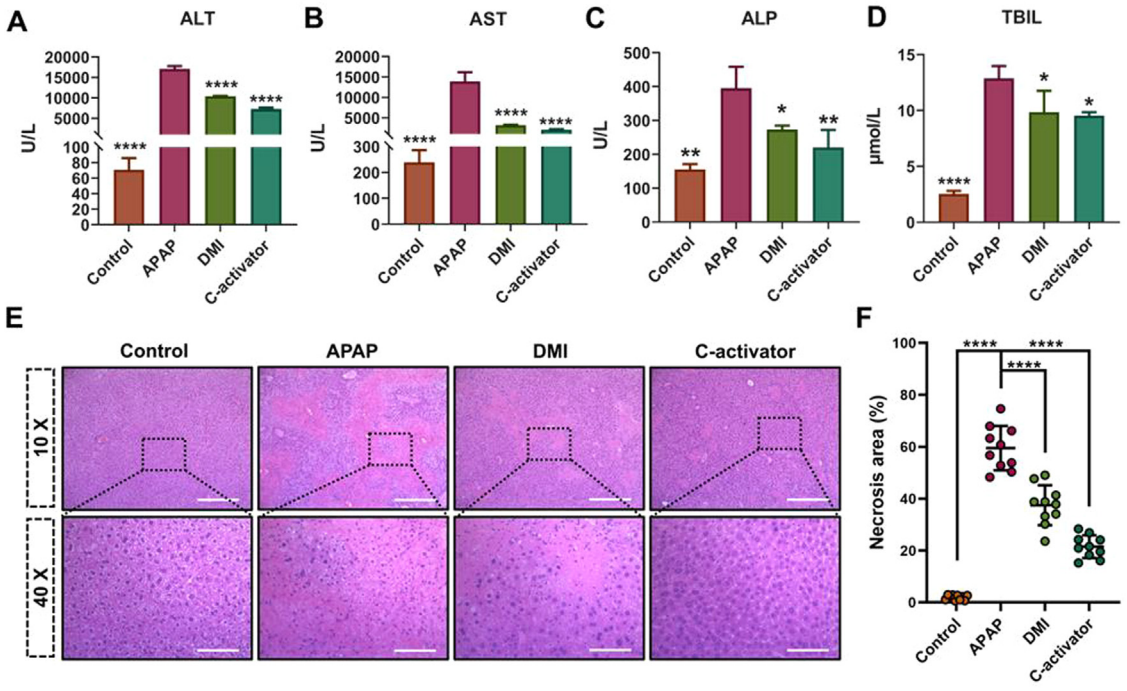

Fig. 6 – Evaluation of C-activator on liver function and histopathology examination. (A-D) Serum biochemical parameters of liver function (A) ALT, (B) AST, (C) ALP and (D) TBIL were analyzed ($n = 3$; mean ± SD). (E) Representative images of H&E-stained livers. Scale bars: 400 μm, top; 100 μm, bottom. (F) Quantification of liver necrosis areas by ImageJ analysis ($n = 10$; mean ± SD). *$P < 0.05$, **$P < 0.01$, ****$P < 0.0001$ compared with APAP group by one-way ANOVA test.

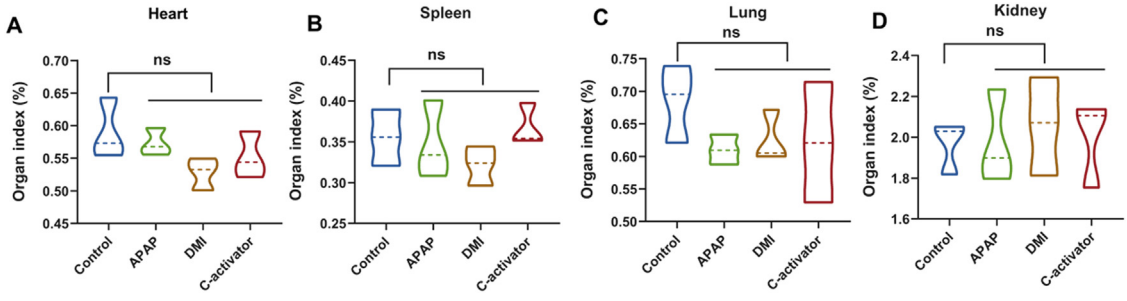

Fig. 7 – *In vivo* safety assessment of C-activator. (A-D) Organ indexes of (A) heart, (B) spleen, (C) lung and (D) kidney after various treatments ($n = 3$; mean ± SD). ns is $P > 0.05$ compared with control group by one-way ANOVA test.

results showed that the liver from APAP-treated mice was characterized by hepatocyte dilation, centrilobular cell death, inflammatory cell infiltration and necrosis. DMI treatment resulted in a certain degree of reduction in the damage and necrosis. On the contrary, the cocktail activator treatment could notably suppress the damage and necrosis in APAP-induced ALF mice (Fig. 6E). Moreover, the decreased liver necrosis area as quantified by H&E staining further confirmed the superior effectiveness of the cocktail activator treatment on ALF (Fig. 6F). Considering safety of liposomes for biological and clinical uses, the organ index of major organs of mice treated with different formulations were evaluated [53]. Compared with mice in the control group, no dramatical difference was detected in the organ index of each group, suggesting that the cocktail activator did not cause obvious adverse effects in mice (Fig. 7A-7D). Taken together, these results clearly demonstrated the outstanding therapeutic performance and good safety profile of the cocktail activator against ALF.

4. Conclusions

In conclusion, we successfully developed a cocktail activator for the treatment of ALF induced by APAP. The cocktail activator acted directly on hepatocytes to achieve hepatocyte rescue, and at the same time stimulated hepatocytes to express growth factors and repair factors for microenvironment modulation, thereby bursting out a cocktail-like therapeutic effect. In this exclusive delivery system, the cocktail activator protected mice from APAP-induced hepatocyte damage by inhibiting

cell death, oxidative stress and inflammatory response of hepatocytes. Furthermore, microenvironment of the cocktail activator-treated hepatocytes could be beneficial to hepatocyte regeneration by promoting the expression of hepatocyte growth factor. Meanwhile, changes in tissue microenvironment caused by the cocktail activator could validly revert activated macrophages to the anti-inflammatory state, reduce the expression of pro-inflammatory cytokines and increase the expression of anti-inflammatory cytokines. More importantly, in APAP-induced ALF mouse model, the cocktail activator exhibited superior therapeutic efficacy to suppress liver injury biomarkers, MDA content and necrosis without causing any side effects. Consequently, all these results imply that the cocktail activator may be a promising candidate for the clinical treatment of ALF.

Conflicts of interest

The authors declare no competing financial interest.

Acknowledgement

This work was supported by National Natural Science Foundation of China (Project No. 81872805, 82073771, 82104085), and Guangdong Basic and Applied Basic Research Foundation (Project No. 2020A1515110147, 2021A1515011418, 2021A1515012025).

Supplementary materials

Supplementary material associated with this article can be found, in the online version, at doi:10.1016/j.ajps.2022.10.001.

REFERENCES

[1] Bernal W, Wendon J. Acute liver failure. N Engl J Med 2013;369(26):2525–34.
[2] Stravitz RT, Lee WM. Acute liver failure. Lancet 2019;394(10201):869–81.
[3] Björnsson ES. Drug-induced liver injury: an overview over the most critical compounds. Arch Toxicol 2015;89(3):327–34.
[4] Dahlin DC, Miwa GT, Lu AY, Nelson SD. N-acetyl-p-benzoquinone imine: a cytochrome p-450-mediated oxidation product of acetaminophen. Proc Natl Acad Sci U S A 1984;81(5):1327–31.
[5] Krenkel O, Mossanen JC, Tacke F. Immune mechanisms in acetaminophen-induced acute liver failure. Hepatobiliary Surg Nutr 2014;3(6):331–43.
[6] McGill MR, Sharpe MR, Williams CD, Taha M, Curry SC, Jaeschke H. The mechanism underlying acetaminophen-induced hepatotoxicity in humans and mice involves mitochondrial damage and nuclear DNA fragmentation. J Clin Invest 2012;122(4):1574–83.
[7] Kubes P, Mehal WZ. Sterile inflammation in the liver. Gastroenterology 2012;143(5):1158–72.
[8] Woolbright BL, Jaeschke H. Sterile inflammation in acute liver injury: myth or mystery? Expert Rev Gastroenterol Hepatol 2015;9(8):1027–9.
[9] Moustafa AHA, Ali EMM, Mohamed TM, Abdou HI. Oxidative stress and thyroid hormones in patients with liver diseases. Eur J Intern Med 2009;20(7):703–8.
[10] Sutti S, Tacke F. Liver inflammation and regeneration in drug-induced liver injury: sex matters!. Clin Sci 2018;132(5):609–13.
[11] Jaeschke H, Ramachandran A. Reactive oxygen species in the normal and acutely injured liver. J Hepatol 2011;55(1):227–8.
[12] Zhan C, Lin G, Huang Y, Wang Z, Zeng F, Wu S. A dopamine-precursor-based nanoprodrug for in-situ drug release and treatment of acute liver failure by inhibiting nlrp3 inflammasome and facilitating liver regeneration. Biomaterials 2021;268:120573.
[13] Cichoż-Lach H, Michalak A. Oxidative stress as a crucial factor in liver diseases. World J Gastroenterol 2014;20(25):8082–91.
[14] Zhang J, Chan HF, Wang H, Shao D, Tao Y, Li M. Stem cell therapy and tissue engineering strategies using cell aggregates and decellularized scaffolds for the rescue of liver failure. J Tissue Eng 2021;12:2041731420986711.
[15] Bambouskova M, Gorvel L, Lampropoulou V, Sergushichev A, Loginicheva E, Johnson K, et al. Electrophilic properties of itaconate and derivatives regulate the iκbζ–atf3 inflammatory axis. Nature 2018;556(7702):501–4.
[16] Mills EL, Ryan DG, Prag HA, Dikovskaya D, Menon D, Zaslona Z, et al. Itaconate is an anti-inflammatory metabolite that activates nrf2 via alkylation of keap1. Nature 2018;556(7699):113–7.
[17] Yi Z, Deng M, Scott MJ, Fu G, Loughran PA, Lei Z, et al. Immune-responsive gene 1/itaconate activates nuclear factor erythroid 2-related factor 2 in hepatocytes to protect against liver ischemia-reperfusion injury. Hepatology 2020;72(4):1394–411.
[18] ElAzzouny M, Tom CT, Evans CR, Olson LL, Tanga MJ, Gallagher KA, et al. Dimethyl itaconate is not metabolized into itaconate intracellularly. J Biol Chem 2017;292(12):4766–9.
[19] Lammers T, Sofias AM, van der Meel R, Schiffelers R, Storm G, Tacke F, et al. Dexamethasone nanomedicines for covid-19. Nat Nanotechnol 2020;15(8):622–4.
[20] Jin Y, Wang H, Yi K, Lv S, Hu H, Li M, et al. Applications of nanobiomaterials in the therapy and imaging of acute liver failure. Nanomicro Lett 2020;13(1):25.
[21] Bhave VS, Paranjpe S, Bowen WC, Donthamsetty S, Bell AW, Khillan JS, et al. Genes inducing ips phenotype play a role in hepatocyte survival and proliferation *in vitro* and liver regeneration *in vivo*. Hepatology 2011;54(4):1360–70.
[22] Fausto N. Liver regeneration. J Hepatol 2000;32(1 Suppl):19–31.
[23] Michalopoulos GK. Hepatostat: liver regeneration and normal liver tissue maintenance. Hepatology 2017;65(4):1384–92.
[24] Albrecht JH. Met and epidermal growth factor signaling: the pillars of liver regeneration? Hepatology 2016;64(5):1427–9.
[25] Liu J, Hu X, Chen J, Li X, Wang L, Wang B, et al. Pericentral hepatocytes produce insulin-like growth factor-2 to promote liver regeneration during selected injuries in mice. Hepatology 2017;66(6):2002–15.
[26] Gatzidou E, Kouraklis G, Theocharis S. Insights on augmenter of liver regeneration cloning and function. World J Gastroenterol 2006;12(31):4951–8.
[27] Mosser DM, Edwards JP. Exploring the full spectrum of macrophage activation. Nat Rev Immunol 2008;8(12):958–69.
[28] Wu Y, Yi L, Li E, Li Y, Lu Y, Wang P, et al. Optimization of glycyrrhiza polysaccharide liposome by response surface

methodology and its immune activities. Int J Biol Macromol 2017;102:68–75.
[29] Cheng MH, Weng JY, Chuang CH, Liao WT, Lai YF, Liu JY, et al. Prolonging the half-life of histone deacetylase inhibitor belinostat via 50 nm scale liposomal subcutaneous delivery system for peripheral t-cell lymphoma. Cancers (Basel) 2020;12(9).
[30] Allen TM, Everest JM. Effect of liposome size and drug release properties on pharmacokinetics of encapsulated drug in rats. J Pharmacol Exp Ther 1983;226(2):539.
[31] Gaumet M, Vargas A, Gurny R, Delie F. Nanoparticles for drug delivery: the need for precision in reporting particle size parameters. Eur J Pharm Biopharm 2008;69(1):1–9.
[32] Qin C, Lv Y, Xu C, Li J, Yin L, He W. Lipid-bilayer-coated nanogels allow for sustained release and enhanced internalization. Int J Pharm 2018;551(1):8–13.
[33] Fan Q, Zhang Y, Hou X, Li Z, Zhang K, Shao Q, et al. Improved oral bioavailability of notoginsenoside r1 with sodium glycocholate-mediated liposomes: preparation by supercritical fluid technology and evaluation *in vitro* and *in vivo*. Int J Pharm 2018;552(1):360–70.
[34] Lin Z, Wu F, Lin S, Pan X, Jin L, Lu T, et al. Adiponectin protects against acetaminophen-induced mitochondrial dysfunction and acute liver injury by promoting autophagy in mice. J Hepatol 2014;61(4):825–31.
[35] Lv H, Yang H, Wang Z, Feng H, Deng X, Cheng G, et al. Nrf2 signaling and autophagy are complementary in protecting lipopolysaccharide/d-galactosamine-induced acute liver injury by licochalcone a. Cell Death Dis 2019;10(4):313.
[36] Yang R, Miki K, He X, Killeen ME, Fink MP. Prolonged treatment with n-acetylcystine delays liver recovery from acetaminophen hepatotoxicity. Critical Care 2009;13(2):R55.
[37] Woolbright BL, Jaeschke H. Role of the inflammasome in acetaminophen-induced liver injury and acute liver failure. J Hepatol 2017;66(4):836–48.
[38] Tanaka N, Ikeda Y, Ohta Y, Deguchi K, Tian F, Shang J, et al. Expression of keap1–nrf2 system and antioxidative proteins in mouse brain after transient middle cerebral artery occlusion. Brain Res 2011;1370:246–53.
[39] Thimmulappa RK, Lee H, Rangasamy T, Reddy SP, Yamamoto M, Kensler TW, et al. Nrf2 is a critical regulator of the innate immune response and survival during experimental sepsis. J Clin Invest 2006;116(4):984–95.
[40] Wei Y, Gong J, Yoshida T, Eberhart CG, Xu Z, Kombairaju P, et al. Nrf2 has a protective role against neuronal and capillary degeneration in retinal ischemia-reperfusion injury. Free Radic Biol Med 2011;51(1):216–24.
[41] Zhang YK, Yeager RL, Tanaka Y, Klaassen CD. Enhanced expression of nrf2 in mice attenuates the fatty liver produced by a methionine- and choline-deficient diet. Toxicol Appl Pharmacol 2010;245(3):326–34.
[42] Morito N, Yoh K, Itoh K, Hirayama A, Koyama A, Yamamoto M, et al. Nrf2 regulates the sensitivity of death receptor signals by affecting intracellular glutathione levels. Oncogene 2003;22(58):9275–81.
[43] Enomoto A, Itoh K, Nagayoshi E, Haruta J, Kimura T, O'Connor T, et al. High sensitivity of nrf2 knockout mice to acetaminophen hepatotoxicity associated with decreased expression of are-regulated drug metabolizing enzymes and antioxidant genes. Toxicol Sci 2001;59(1):169–77.
[44] Tacke F, Trautwein C. Mechanisms of liver fibrosis resolution. J Hepatol 2015;63(4):1038–9.
[45] Liu L, Yannam GR, Nishikawa T, Yamamoto T, Basma H, Ito R, et al. The microenvironment in hepatocyte regeneration and function in rats with advanced cirrhosis. Hepatology 2012;55(5):1529–39.
[46] Tacke F. Targeting hepatic macrophages to treat liver diseases. J Hepatol 2017;66(6):1300–12.
[47] Lawrence T, Natoli G. Transcriptional regulation of macrophage polarization: enabling diversity with identity. Nat Rev Immunol 2011;11(11):750–61.
[48] Weber C. Alternatively activated macrophages mediate fibrosis. Nat Rev Gastroenterol Hepatol 2015;12(7):372 -72.
[49] Zhu L, Yang T, Li L, Sun L, Hou Y, Hu X, et al. Tsc1 controls macrophage polarization to prevent inflammatory disease. Nat Commun 2014;5:4696.
[50] Walker RM, Massey TE, McElligott TF, Racz WJ. Acetaminophen toxicity in fed and fasted mice. Can J Physiol Pharmacol 1982;60(3):399–404.
[51] Wang J, Qiao L, Li Y, Yang G. Ginsenoside rb1 attenuates intestinal ischemia-reperfusion- induced liver injury by inhibiting nf-kappab activation. Exp Mol Med 2008;40(6):686–98.
[52] Moseley RH. Evaluation of abnormal liver function tests. Med Clin North Am 1996;80(5):887–906.
[53] Guo L, Zhang Y, Wei R, Wang C, Feng M. Lipopolysaccharide-anchored macrophages hijack tumor microtube networks for selective drug transport and augmentation of antitumor effects in orthotopic lung cancer. Theranostics 2019;9(23):6936–48.